Synthetic aperture imaging radar signal simulation of urban environments

Thomas Stenson Moffat
11501

MEng final individual project report

Academic Year 2020-2021
Dr Robert Watson
Wordcount:

Abstract

Contents

List of Figures

List of Symbols

A_e	Effective antenna aperture area
B	Bandwidth of the signal
D	Aperture size in desired dimension
ΔR	Radial resolution
Δr	Difference between r and r_0
ΔR_g	Ground resolution
Δx	Cross-range resolution
G	Total gain
k	Boltzmann's constant
k_0	Angular wave number (i.e. $\frac{2\pi}{r}$)
λ	Wavelength of the signal
n	A number
P_{av}	Average power across all pulses
$\phi(x)$	2-way phase history
P_n	Noise power
P_t	Transmitter power
R	Range
r	Outer radial distance of the beam
r_0	Center distance of the beam
$R_{\max}$	Maximum range
σ^0	Noise equivalent
σ_b	Radar cross-section
θ_{sa}	Synthesised beam width
T_{obs}	Time spent observing the target
T_{sys}	System noise temperature
v_p	Platform velocity
x	Total displacement of the platform

Part 1

Introduction

Part 2

Engineering Analysis

2.1 Introduction to SAR

Synthetic aperture radar (SAR) is a method of radar imaging that allows for a greater dimension of radar aperture than is possible in a single element or an array of elements. This is generally achieved by mounting a radar transceiver to a moving platform and moving it past the target to be imaged however the transceiver can be stationary and the target moved past it. The image uses the relative movement between the platform and the target to build up an image based on the responses received and then time multiplexing all the responses. This movement, and hence the larger aperture created, allows for a finer spatial resolution than can be achieved by more conventional beam scanning radar. These images can be useful for a variety of applications such as remote mapping of the surface of the Earth for glaciology and geology among others. Interferometric SAR can also be used to create elevation maps by taking two measurements from different positions and comparing the differences. Simulating a SAR image is desirable as flight time can be expensive and time consuming to get quality images so defining the flight paths and angles before any imaging is carried out saves both time and money.

There are two main methods of imaging using SAR. These are stripmap and spotlight imaging. Stripmap imaging SAR keeps the radar beam fixed at 90°to the direction of travel of the platform to which it is mounted, giving an even resolution image over the entire imaging area. Spotlight SAR uses beam steering in order to focus on one specific area to increase image resolution in that area, at the expense of image resolution in other areas. This extra time spent focusing on the single area increases the synthetic aperture length for that section only which increases the resolution.

The SAR radar equation

There are two main approaches to SAR, focused and unfocused SAR. These differ in how they consider shifts in the response phase, as focused SAR only takes into account the Doppler shift across the aperture, while focused SAR takes into account the phase shift

(a) SAR in stripmap operation

(b) SAR in spotlight operation

Figure 2.1: The two main modes of operation of SAR, reproduced from [1]

in the beam due to the change in range caused by the target passing through the beam. This means that the resolution of the image is determined by the length of the entire synthetic aperture, as opposed to in unfocused SAR where the resolution is a function of the shortest range between the platform and the target as well as the wavelength of the signal. The resolution of focused SAR is wavelength independent. The derivation of this can be found in Appendix A. Also in this appendix is a derivation of the radar equation both generally and then to the more specific version for SAR. The more general form of the radar equation for a single pulse is given as

$$\text{SNR} = \frac{P_t G^2 \lambda^2 \sigma_b}{(4\pi)^3 R^4 k T_{sys} B} = \frac{P_t A_e^2 \sigma_b}{4\pi \lambda^2 k T_{sys} B R^4}$$

which gives the signal-to-noise ratio for a single pulse, where P_t is the transmitted power, G is the gain of the system, A_e is the effective aperture area, λ is the wavelength of the signal, σ_b is the radar cross-section, R is the signal range, k is Boltzmann's constant, T_{sys} is the system noise temperature and B is the bandwidth of the system. This can then be adapted to the SAR-specific radar equation by increasing the number of pulses n to give

$$\text{SNR} = \frac{P_t A_e^2 \sigma_b n}{4\pi \lambda^2 k T_{sys} B R^4}$$

and hence the signal-to-noise ratio of a distributed target is given by

$$\text{SNR} = \frac{P_{av} A_e^2 \sigma^0 \Delta R_g \Delta x t_{obs}}{4\pi \lambda^2 k T_{sys} R^4} \text{ or } \text{SNR} = \frac{P_{av} A_e^2 \sigma^0 \Delta x \lambda^3}{(4\pi)^3 R^3 k T_{sys} 2 v_p}$$

where P_{av} is the average power across all pulses, ΔR_g is the ground range resolution of the system, T_{obs} is the observation time of the target and v_p is the platform velocity. The sensitivity of a SAR system can be expressed as the noise equivalent σ^0, which is the value of σ^0 at the maximum range to give a signal-to-noise ratio of 1 (or 0 dB) [2].

SAR Image Artefacts

There are a few artefacts that can arise as part of SAR imagery (and radar imagery in general). Some of these, such as range ambiguities, aren't relevant in this case due to the fact that all the targets being imaged are static and this is only a real issue in moving objects. Some artefacts will need to be considered though. The first of these is speckle, which is a result of the fact that the energy arriving at the pixel is pretty coherent, so it has a single phase on arrival at said pixel. Generally the pixel will be the sum of multiple scatterers as opposed to one single scatterer, meaning that it is likely to be affected by background reflections and so result in a relatively noisy image. This can be fixed in real world applications by splitting the SAR antenna into multiple sections and take the same image with each section. This then allows for the pixel values to be averaged out, hopefully removing the speckle at the cost of some resolution [3].

Another image artefact that will need to be considered can be caused by strong scatterers that means that the signal is reflected multiple times before returning to the receiver. This can be seen most strongly with a bridge over water as it involves both a hard target in the bridge and a dihedral reflection from the water. This mostly occurs when the target is aligned with the path of the platform and the multiple reflections can cause the bridge to appear multiple times in the image due to the multiple bounces taken by the signal increase the Doppler shift presented when it is filtered on reception. The same signal is in essence received multiple times and so the algorithm reads it as different displacements for the same target [3].

Finally, some distortions can be created due to the geometry of the radar beam. Targets nearer the platform can appear compressed on the output image as the ground range in that location is greater but in the final image is represented in the same amount of image space as targets further away. Similarly, given a tower, reflections from the top of the tower will return to the platform before reflections from the bottom, causing the tower to appear to lean over towards the radar [3].

2.2 Literature Review

2.2.1 A Summary of Methods Previously Explored in Literature

The table that follows summarises the methods used in literature and a brief list of advantages and disadvantages. An in-depth exploration of the papers used can be found in section 2.2.2 and an exploration of each possible method and their suitability for this project can be found in section 3.1.

Method	Advantages	Disadvantages
Raw signal	The most accurate method of simulation available as it uses the characteristics of the radar beam in order to simulate the responses of the structures it reflects off.	Most computationally complex method as it has to simulate the effects of every beam every time a pulse is transmitted and received.
Rasterisation	The fastest method of simulating SAR as it uses image transformation techniques in order to give a good idea of how an image will look, this method is capable of real-time updates of the image which means it has applications in SAR data capture planning.	The least accurate method as it is only performing an image transform as opposed to a full simulation of the signal.
Ray tracing	A good balance of speed and accuracy, uses advanced computer graphics techniques to only simulate the parts of the model available to the observer so is less computationally intense than the raw signal but also more accurate than rasterisation.	Requires a good graphics processor as well as a good modelling environment in which to perform it, this is by far the most complex to implement from scratch
Hybrid methods	Has the potential to be a good balance between the raw signal and ray tracing as it uses raw signal for the higher order contributions and ray tracing for the more obvious single reflections	This is the least explored method so very few conclusions about its actual performance can be drawn, with only one paper found that uses it.

2.2.2 In-Depth Findings

Raw SAR Simulation

There are three main methods that have previously been explored for simulating SAR. The first of these, which is the most accurate is simulating the effects of the beam itself,

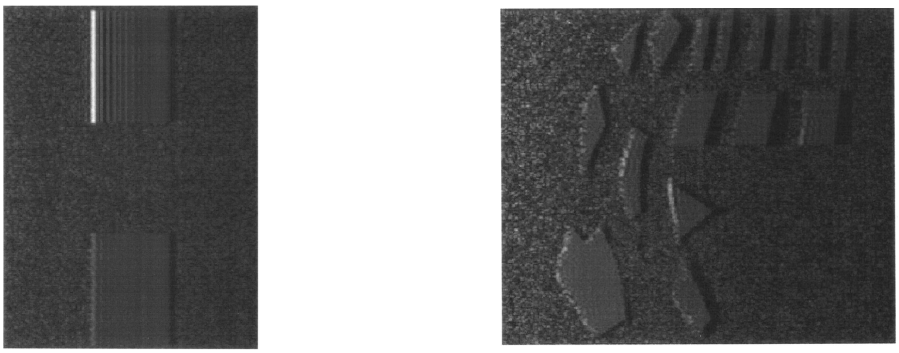

(a) Simulated single-look SAR with two buildings (b) Simulated single-look SAR with 16 buildings

Figure 2.2: Simulated SAR images from Franceschetti *et al.* 2003 [4]

as detailed in Franceschetti *et al.* 2003 [4]. This describes creating the raw data as would be expected in a SAR system in the real world and then transforming it to create a SAR image. The ground work for this was laid in Franceschetti *et al.* 1992 [5], which itself builds on Francescetti and Schirinzi's work on a SAR processor based on two-dimensional FFT codes [6]. This approach has the advantages of being able to take into account backscattering as well as the higher-order signal contributions created by scattering as the signal reflects off of both a wall and the ground. A lot of the preliminary work with regards to the behaviour of electromagnetic backscattering was conducted in [7]. This describes a model that allows for the return from a structure to a microwave sensor to be analysed and so determine its dielectric properties as well as its geometric properties. The optics can be altered to simulate the roughness of the surface the signal is reflected off of last before it is received by the sensor. This can also be expanded to simulate backscattering. This simulator as a whole works very well with individual objects, however the simulation time was found to scale linearly with the number of objects present in the scene. Simulations in [4] were carried out using a Pentium IV processor from Intel Corp, released in 2001 which means that the simulation times achieved are not necessarily reflective of the performance achievable on more modern processors, however at the time it was found that while one object in a 512x512 pixel image required approximately 34 seconds, two objects in the same sized image required 1'02" and 16 objects increased this computation time up to 7'38". This is not ideal if the aim is real-time or even near real-time simulation capabilities as most urban environments that are to be simulated will contain far more than 16 structures. This efficiency does seem to have been improved in Franceschetti *et al.* 2007 [8] as in this paper it is used to simulate a SAR image of a $400 \times 600\text{m}^2$ area of the centre of Munich, incorporating the Technische Universität and the Alta Pinakothek, which leads to a reasonably complicated scene.

A similar approach building on the previously mentioned work is presented by Zheng *et al.* [9] which uses the scattering model in order to accurately simulate a SAR scene. This is achieved by making the assumption that the scene is made up of vertical buildings distributed on a rough dielectric terrain. This also discusses the computation of scattering coefficients under different conditions. As with the previous approach (and the following raw SAR approach) the Kirchhoff approach is used in this case.

A similar approach to robust SAR simulation is described in Dellière *et al.* 2007 [10], which uses an electromagnetic approach closely following Maxwell's equations to create a finite-difference time domain method of simulation, which differs from [4] as that instead manipulates the signal in the frequency domain in order to create the raw SAR signal. This system has similar drawbacks to Franceschetti's approach with regards to computation complexity and time required, but is even more computationally complex,

(a) An actual SAR image of a portion of Munich

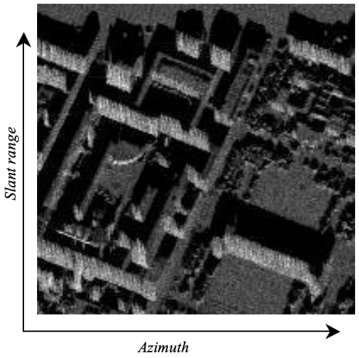

(b) A simulated SAR image of the same area

Figure 2.3: A comparison between an actual SAR image and simulated SAR image of the Technische Universität and Alte Pinakothek from [8]

due to its ability to handle dispersive materials as well as phase changes. This approach could be of some interest for creating an incredibly robust simulator due to the advances in computing performance between the publication date and today.

Graphical SAR Simulation

There are two methods that are less complex computationally for simulating the image achieved by SAR. These both arise from graphics manipulation and more specifically 3 dimensional modelling. These are rasterisation and ray tracing. Rasterisation is the process of taking a 3 dimensional area and creating a 2 dimensional image using some sort of image transformation based on the location of the camera to the object in the 3D area. Ray tracing follows a similar process to light, just in reverse. It sends beams out from the camera in all directions that the camera can see and simulates them reflecting off of objects until they hit a source of illumination. Using this the rendering engine can determine if an object is illuminated or not and adjust appropriately. These two approaches have both been used in the past for simulation of SAR images. Rasterisation was used by Balz 2006 [11] and ray tracing was explored by Auer *et al.* 2008 [12] and Mametsa *et al.* 2002 [13]. This second paper was used in Hammer *et al.* [14] along with Balz 2006 to compare the relative merits of these two approaches. Ultimately the advantages of Balz's approach as detailed in [15] and [11] is that the simulator is real-time so can be used to determine optimal azimuthal directions when recording a SAR image using a physical airborne platform. This form of simulation however doesn't take into account the contributions of higher order reflections so if it is being used for a demonstration tool, the images produced are less representative of an actual SAR image. This also means that corners aren't visible in the image, meaning that this form of simulation can't be used to test feature extraction algorithms. The two ray tracing simulators tested within [14] can simulate these higher-order contributions meaning they can be used to test feature extraction algorithms, however due to the computationally intensive nature of ray tracing these can't be simulated in real time, so this form of simulation is less useful for planning purposes.

All of the forms of simulation presented here so far are only as good as the models used, as generally the modelled buildings are assumed to be made of one material with a fixed dielectric constant, while the modelled ground is made of a different material. In [14], the buildings modelled are created entirely of stone, with a grass ground. In real life however this becomes more complicated as buildings do tend to be made up of multiple materials, and often in urban areas the ground is made up of a material with a similar dielectric

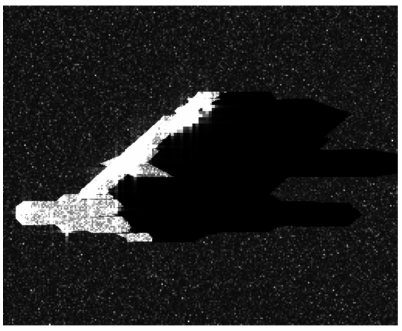

(a) 0.3m resolution simulation of the Stiftskirche in Stuttgart

(b) 5m resolution simulation of Stuttgart

Figure 2.4: Results from Balz 2006 [15] using rasterisation techniques

(a) A reference spotlight image of the Alta Pinakothek

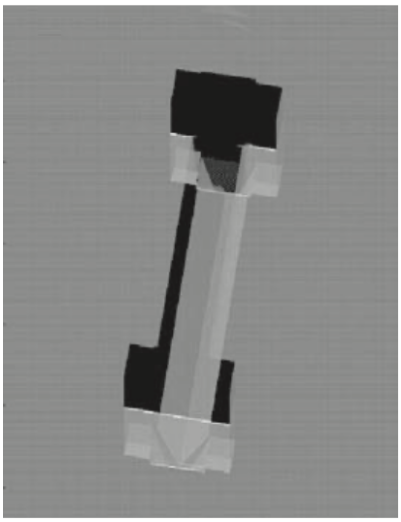

(b) A simulated SAR image using ray tracing of the Alta Pinakothek

Figure 2.5: Simulated SAR using ray tracing from Auer *et al.* 2008 [12]

constant to the buildings. This also doesn't include any forms of dispersive materials such as metal. It is unclear whether any of the simulators covered in [14] can simulate these sorts of materials accurately, which is something that should be taken to account in the future.

Yet another method similar to the image processing approaches is presented by Lu *et al.* [16] and uses methods most commonly used by video games. In this case the raw mathematic SAR simulation is not carried out, similar to [17] and [12] and uses an orthogonal projection to cast the 3D model to a 2D image based on the slant range of the camera. This again has the potential of improving the performance of image generation in incredibly complicated scenes such as city centres.

Hybrid Method and Other Papers of Note

Chen *et al.* 2011 [18] proposes a hybrid method of simulating these images using analytical models. In this approach, the contributions provided by backscattering are shown using an electromagnetic analytical model ultimately based on that described by [4], and the object position vectors are given by a geometric model using ray tracing. In this paper the analysis is mostly focused on cylindrical or cylinder-like buildings, with some analysis devoted to flat-roof buildings as well. This approach has a potential to be more accurate than the ray tracing models proposed previously due to the electromagnetic models involved, but also be less computationally complex than the more canonical SAR image simulators.

Xu and Jin 2006 [19] is a paper that is not immediately relevant to this situation due to it modelling natural environments for SAR simulation however this is potentially interesting and relevant due to the variety of materials present in urban environments to be modelled. This is an algorithm that can deal with randomly and heterogeneously distributed objects within an image with varying dielectric constants and can deal with them in a reasonable length of time. This is something that is worth exploring if there is time in the future as it would add robustness to the system as a whole.

Part 3

Methods

3.1 Exploration of Methods Used and Their Suitability

The four possible methods that can be used in this project are, as mentioned previously, raw signal simulation, rasterisation, ray tracing and a hybrid method. In this section I will cover their suitability as they relate to this project, as well as explore the methods of transforming SAR raw signals into an actual image.

3.1.1 SAR Simulation Methods

Raw SAR Simulation

This is the most robust form of simulation and the most accurate as the individual signals are simulated as well as their reflections. This does have some drawbacks as developing the system in the first place is likely to be quite complex due to the

3.1.2 Image Forming Methods

There are multiple methods of image formation algorithm.

3.2 Results and Outcomes

3.3 Milestones Achieved

Part 4

Deliverables

4.1 Deliverables Achieved

4.2 Significant Results

4.3 Uncertainty

4.4 Final Results

Part 5

Conclusions

5.1 Final Remarks and Outcome

5.2 Further Work

Acknowledgements

Bibliography

[1] C. Wolff. (Apr. 3, 2012). "Synthetic Aperture Radar Modes," Radartutorial, [Online]. Available: https://www.radartutorial.eu/20.airborne/ab08.en.html (visited on 03/12/2021).

[2] R. Watson, "EE40136: Radar Systems and Remote Sensing," Lecture Notes, Lecture Notes, University of Bath, Bath, Sep. 28, 2020.

[3] J. Richards, *Remote Sensing with Imaging Radar*, ser. Signals and Communication Technology. Springer, 2009.

[4] G. Franceschetti, A. Iodice, D. Riccio, and G. Ruello, "SAR raw signal simulation for urban structures," *IEEE Transactions on Geoscience and Remote Sensing*, vol. 41, no. 9, p. 10, 2003.

[5] G. Franceschetti, M. Migliaccio, D. Riccio, and G. Schirinzi, "SARAS: A synthetic aperture radar (SAR) raw signal simulator," *IEEE Transactions on Geoscience and Remote Sensing*, vol. 30, no. 1, pp. 110–123, Jan. 1992, ISSN: 1558-0644. DOI: 10.1109/36.124221.

[6] G. Franceschetti and G. Schirinzi, "A SAR processor based on two-dimensional FFT codes," *IEEE Transactions on Aerospace and Electronic Systems*, vol. 26, no. 2, pp. 356–366, Mar. 1990, ISSN: 1557-9603. DOI: 10.1109/7.53462.

[7] G. Franceschetti, A. Iodice, and D. Riccio, "A canonical problem in electromagnetic backscattering from buildings," *IEEE Transactions on Geoscience and Remote Sensing*, vol. 40, no. 8, pp. 1787–1801, Aug. 2002, ISSN: 1558-0644. DOI: 10.1109/TGRS.2002.802459.

[8] G. Franceschetti, R. Guida, A. Iodice, D. Riccio, G. Ruello, and U. Stilla, "Simulation Tools for Interpretation of High Resolution SAR Images of Urban Areas," in *2007 Urban Remote Sensing Joint Event*, Apr. 2007, pp. 1–5. DOI: 10.1109/URS.2007.371841.

[9] Y. Zheng, B. Zhou, and Z. Zong, "Simulation method of SAR raw echo for urban scene," in *2008 International Conference on Radar*, Sep. 2008, pp. 503–507. DOI: 10.1109/RADAR.2008.4653976.

[10] J. Delliere, H. Maitre, and A. Maruani, "SAR measurement simulation on urban structures using a FDTD technique," in *2007 Urban Remote Sensing Joint Event*, Apr. 2007, pp. 1–8. DOI: 10.1109/URS.2007.371837.

[11] T. Balz, "Real-time SAR simulation of complex scenes using programmable Graphics Processing Units," Jul. 1, 2006.

[12] S. Auer, S. Hinz, and R. Bamler, "Ray Tracing for Simulating Reflection Phenomena in SAR Images," in *IGARSS 2008 - 2008 IEEE International Geoscience and Remote Sensing Symposium*, vol. 5, Jul. 2008, pp. V - 518-V –521. DOI: 10.1109/IGARSS.2008.4780143.

[13] H.-J. Mametsa, F. Rouas, A. Berges, and J. Latger, "Imaging radar simulation in realistic environment using shooting and bouncing rays technique," in *SAR Image Analysis, Modeling, and Techniques IV*, vol. 4543, International Society for Optics and Photonics, Jan. 28, 2002, pp. 34–40. DOI: 10.1117/12.453975.

[14] H. Hammer, T. Balz, E. Cadario, U. Soergel, U. Thoennessen, and U. Stilla, "Comparison of SAR simulation concepts for the analysis of high-resolution SAR data," in *7th European Conference on Synthetic Aperture Radar*, Jun. 2008, pp. 1–4.

[15] T. Balz and N. Haala, "Improved Real-Time SAR Simulation in Urban Areas," in *2006 IEEE International Symposium on Geoscience and Remote Sensing*, Jul. 2006, pp. 3631–3634. DOI: 10.1109/IGARSS.2006.930.

[16] Y. Lu, K. Wang, X. Liu, and W. Yu, "A GPU based real-time SAR simulation for complex scenes," in *2009 International Radar Conference "Surveillance for a Safer World" (RADAR 2009)*, Oct. 2009, pp. 1–4.

[17] T. Balz and U. Stilla, "Hybrid GPU-Based Single- and Double-Bounce SAR Simulation," *IEEE Transactions on Geoscience and Remote Sensing*, vol. 47, no. 10, pp. 3519–3529, Oct. 2009, ISSN: 1558-0644. DOI: 10.1109/TGRS.2009.2022326.

[18] H. Chen, Y. Zhang, K. Tang, W. Xiong, and C. Ding, "Radar imaging simulation for typical urban structures based on analytical models," in *Proceedings of 2011 IEEE CIE International Conference on Radar*, vol. 2, Oct. 2011, pp. 1362–1365. DOI: 10.1109/CIE-Radar.2011.6159811.

[19] F. Xu and Y. Jin, "Imaging Simulation of Polarimetric SAR for a Comprehensive Terrain Scene Using the Mapping and Projection Algorithm," *IEEE Transactions on Geoscience and Remote Sensing*, vol. 44, no. 11, pp. 3219–3234, Nov. 2006, ISSN: 1558-0644. DOI: 10.1109/TGRS.2006.879544.

Appendix A

Derivations

A.1 Focused SAR Resolution

A.1.1 Along track resolution

$$r = r_0 + \Delta r \tag{A.1}$$

$$\Delta r = (r_0^2 + x^2)^{\frac{1}{2}} - r_0 \tag{A.2}$$

$$\Delta r \approx \frac{x^2}{2r_0} \tag{A.3}$$

$$\phi(x) = -2k_0\Delta r = -\frac{2\pi x^2}{\lambda r_0} \tag{A.4}$$

$$\theta_{sa} \approx \frac{\lambda}{2L_s} \tag{A.5}$$

$$\Delta x = \theta_{sa} r_0 \tag{A.6}$$

$$\Delta x = \frac{\lambda}{2L_s} r_0 = \frac{\lambda}{2r_0 \frac{\lambda}{D}} r_0 \tag{A.7}$$

$$\Rightarrow \Delta x = \frac{D}{2} \tag{A.8}$$

In this case, r is the outer radial distance of the beam, r_0 is the center distance of the beam, Δr is the difference between these two distances, x is the distance travelled by the platform over the time measured, k_0 is the angular wave number of the signal, $\phi(x)$ is the two-way phase history of the signal, λ is the wavelength of the signal, θ_{sa} is the synthesised beam width obtained after azimuth processing, Δx is the resolution of the system and D is the aperture size in the chosen dimension (i.e. here it's the azimuthal dimension). Derivation from [3] and [2].

A.1.2 Down-range resolution

With the assumption made that there is some form of pulse compression on the signal we have a radial resolution of

$$\Delta R = \frac{c}{2B}$$

and by geometry we get a ground resolution of

$$\Delta R_g = \frac{c}{2B\sin(\theta)}$$

so to avoid any range ambiguities,

$$\frac{c}{2R_{max}} > \text{PRF}$$

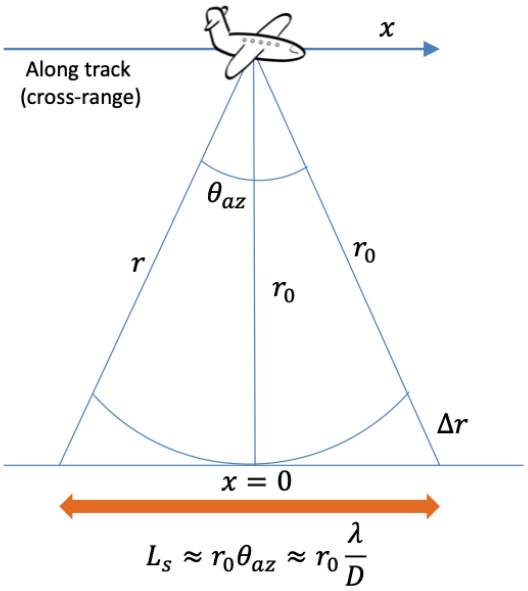

Figure A.1: Along-track/Cross-range SAR Resolution, reproduced from [2]

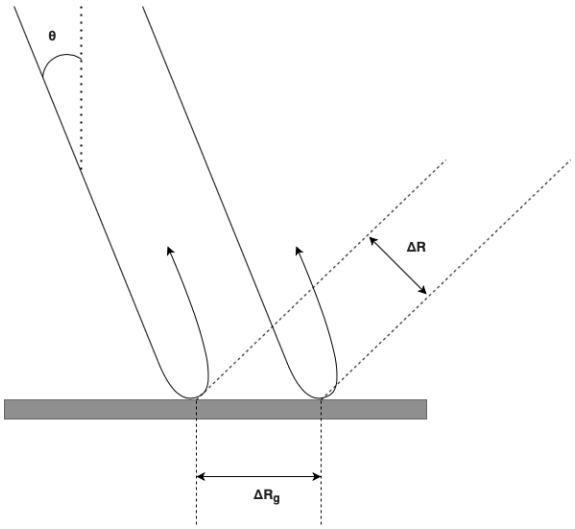

Figure A.2: Down-range SAR resolution, adapted from [3]

where $R_{\max}$ is the maximum range achievable by the radar, ΔR_g is the ground range resolution and ΔR is the radial resolution of the signal.

A.2 Derivation of the Radar Equation

Again derivations from [3] and [2].

$$\text{Isotropic Antenna Power Density} = \frac{P_t}{4\pi R^2} \tag{A.9}$$

$$\text{Directive Antenna Power Density} = \frac{P_t G_t}{4\pi R^2} \tag{A.10}$$

$$\text{Power Intercepted by Target} = \frac{P_t G_t}{4\pi R^2}\sigma_b \tag{A.11}$$

$$\text{Power density at receiver} = \frac{P_t G_T}{4\pi R^2}\sigma_b \times \frac{1}{4\pi R^2} \tag{A.12}$$

$$P_r = \frac{P_t G_t}{4\pi R^2}\sigma_b \times \frac{1}{4\pi R^2} \times A_e \tag{A.13}$$

$$G_r = \frac{4\pi}{\lambda^2} A_e \tag{A.14}$$

$$G_t = G_r = G \tag{A.15}$$

$$\Rightarrow P_r = \frac{P_t G^2 \lambda^2}{(4\pi)^3 R^4}\sigma_b \tag{A.16}$$

Noise power P_n is given by $P_n = kT_{sys}B$ and so the equation for SNR is given as

$$\frac{P_r}{P_n} = \frac{P_t G^2 \lambda^2 \sigma_b}{(4\pi)^3 R^4 k T_{sys} B}$$

and so the radar equation for a distributed target is given by

$$\sigma_b = \sigma^0 \Delta R_g \Delta x \tag{A.17}$$

$$\Delta x = \frac{R\lambda}{2L_s} = \frac{D}{2} \tag{A.18}$$

$$\Delta R_g = \frac{c}{2B\sin(90^\circ - \alpha)} \tag{A.19}$$

$$t_{obs} = nT_s = \frac{L_s}{v_p} \tag{A.20}$$

$$n = \frac{L_s}{T_s v_p} \tag{A.21}$$

$$P_t = \frac{P_{av} T_s}{\tau} \tag{A.22}$$

$$\tau B \approx 1 \tag{A.23}$$

$$\text{SNR} = \frac{P_{av} A_e^2 \sigma^0 \Delta R_g \Delta x t_{obs}}{4\pi\lambda^2 k T_{sys} R^4} \text{or} \text{SNR} = \frac{P_{av} A_e^2 \sigma^0 \Delta x \lambda^3}{(4\pi)^3 R^3 k T_{sys} 2 v_p} \tag{A.24}$$